

Fall 2022

## Effect of Passive Clean Air Injection Into the Wake Region of a Moving Ground Vehicle

Angelos Kaminis

Embry-Riddle Aeronautical University, kaminisa@my.erau.edu

Follow this and additional works at: <https://commons.erau.edu/edt>



Part of the [Automotive Engineering Commons](#), and the [Other Mechanical Engineering Commons](#)

---

### Scholarly Commons Citation

Kaminis, Angelos, "Effect of Passive Clean Air Injection Into the Wake Region of a Moving Ground Vehicle" (2022). *Doctoral Dissertations and Master's Theses*. 694.

<https://commons.erau.edu/edt/694>

This Thesis - Open Access is brought to you for free and open access by Scholarly Commons. It has been accepted for inclusion in Doctoral Dissertations and Master's Theses by an authorized administrator of Scholarly Commons. For more information, please contact [commons@erau.edu](mailto:commons@erau.edu).

EFFECT OF PASSIVE CLEAN AIR INJECTION INTO THE WAKE REGION OF A  
MOVING GROUND VEHICLE

by

Angelos Kaminis

A Thesis Submitted to the College of Engineering Department of Mechanical  
Engineering in Partial Fulfillment of the Requirements for the Degree of  
Master of Science in Mechanical Engineering

Embry-Riddle Aeronautical University  
Daytona Beach, Florida  
November 2022

EFFECT OF PASSIVE CLEAN AIR INJECTION INTO THE WAKE REGION OF A  
MOVING GROUND VEHICLE

by

Angelos Kaminis

This thesis was prepared under the direction of the candidate's Thesis Committee Chair, Dr. Boetcher S., Daytona Beach Campus, and Thesis Committee Members Dr. Hockley C, Daytona Beach Campus, and Dr. Compere M, Daytona Beach Campus, and has been approved by the Thesis Committee. It was submitted to the Department of Mechanical Engineering in partial fulfillment of the requirements for the degree of Master of Science in Mechanical Engineering

Thesis Review Committee:

---

Sandra. Boetcher, Ph.D.  
Committee Chair

---

Christopher. Hockley, Ph.D.  
Committee Member

---

Marc. Compere, Ph.D  
Committee Member

---

Jean-Michel Dhainaut, Ph.D.  
Graduate Program Coordinator,  
Mechanical Engineering

---

Patrick. Currier, Ph.D.  
Department Chair,  
Mechanical Engineering

---

Gregory James, Ph.D.  
Dean, College of Engineering

---

Christopher Grant, Ph.D.  
Associate Vice President of Academics

---

Date

## **Acknowledgements**

I would like to acknowledge my advisor Dr Sandra Boetcher, for being helpful and understanding when life threw curveballs my way, and whose advice and knowledge were invaluable when putting the pieces together and forming this project.

I would also like to thank my brother George, as without him my studies would not have been possible. He has always supported me in my studies, motivated and believed in me even when times were rough. I want to thank my wife Sophie for her tremendous support and motivation, who helped me stay on task and keep my eyes on the goal. She pushed me when I needed to be motivated, but also reminded me that its ok to take a day for myself. Without her the mental toll of the last few years would have been tremendous. I would like to also thank my parents, who have been an amazing support and have sacrificed a lot for me to be here.

Last but not least I would like to thank Embry-Riddle Aeronautical University for providing me with such amazing opportunities, a great education, and very talented and knowledgeable faculty.

## Abstract

Researcher: Angelos Kaminis

Title: EFFECT OF PASSIVE CLEAN AIR INJECTION INTO THE WAKE REGION OF A MOVING GROUND VEHICLE

Institution: Embry-Riddle Aeronautical University

Degree: Master of Science in Mechanical Engineering

Year: 2022

The wake region on a moving ground vehicle is responsible for 70% of the aerodynamic drag when the speed of 90km/h is achieved. The topic of wake region manipulation has been revisited multiple times and with varying techniques. When manipulating the flow utilizing a fully passive method, pressure drag can be reduced, increasing the overall performance of the vehicle. To ensure high velocity fluid injection, a venturi shaped roof was implemented with an inlet size of 352mm x 12.7mm, and 2 outlets of size 88.011mm x 25.4mm resulting in an area of  $4,470.959 \text{ mm}^2$  for both inlet and outlet to maintain conservation of mass and not increase the pressure build up. These outlets were placed at the top corners of the rear window. This resulted in a net drag reduction of 11% from the base model simulation and a reduction of 5.78% from experimental data. The C-pillar vortex was reduced in size and pushed further out of the wake region as the overall pressure increased creating a smaller pressure difference. This suggests that passive clear air injection is a valid method in reducing pressure drag. This concept can be implemented on any object moving through a fluid, reducing pressure drag, increasing efficiency, and reducing fuel consumption on vehicles.

## Table of Contents

Acknowledgements.....	ii
List of Tables .....	vi
Nomenclature .....	x
Chapter I.....	1
Introduction .....	1
Chapter II .....	7
Literature Review .....	7
Past methods of wake manipulation.....	8
Venturi concept .....	10
Chapter III.....	12
Methodology .....	12
Passive air injection solution.....	12
CAD setup.....	14
CFD analysis .....	17
Mesh independent study .....	19
Chapter IV.....	22
Discussion, Conclusion, and Recommendations.....	22
Recommendations .....	43
References.....	44



## **List of Tables**

Table 1 Enclosure Parameters.....	15
Table 2 Mesh Independent Study .....	20
Table 3 CFD Results.....	22

## List of Figures

Figure 1 DrivAer model and Ahmed body pillar locations .....	5
Figure 2 C-pillar vortex distribution, (Rositto G, et al. 2016) .....	6
Figure 3 wake region breakdown, (Rositto G, et al. 2016).....	6
Figure 4 Venturi design (Bashir A. 2011) .....	11
Figure 5 Inlet location .....	13
Figure 6 Basic Ahmed Body CAD setup .....	15
Figure 7 Basic Ahmed body CAD .....	15
Figure 8 Design 1 design .....	16
Figure 9 Design 2 implementation.....	17
Figure 10 Mesh independent study results.....	19
Figure 11 Enclosure and BOI Mesh.....	20
Figure 12 Close up of BOI and body surface mesh .....	22
Figure 13 Pressure Contour of base model side profile .....	23
Figure 14 Pressure Contour of design 1 side profile.....	23
Figure 15 Pressure contour of design 2 side profile .....	24
Figure 16 Location of pressure contour for figures 17-19.....	24
Figure 17 Pressure Contour at rear of base Ahmed model .....	25
Figure 18 Pressure Contour at the rear of Design 1 .....	25
Figure 19 Pressure contour at the rear of Design 2.....	26
Figure 20 Location of pressure contour for figures 21-23.....	26
Figure 21 Pressure Contour 0.5m behind the base Ahmed model.....	27
Figure 22 Pressure Contour 0.5m behind Design 1 .....	27
Figure 23 Pressure contour 0.5m behind Design 2 .....	22

Figure 24 Top-down pressure contour of Ahmed model at half height.....	22
Figure 25 Top-down pressure contour of Design 1 at half height .....	29
Figure 26 Top-down pressure contour of design 2 at half height.....	29
Figure 27 Top-down pressure contour of base Ahmed model at 0.2m height.....	30
Figure 28 Top-down pressure contour of design 1 at 0.2m height .....	31
Figure 29 Top-down pressure contour of design 2 at 0.2m height .....	32
Figure 30 location of pressure contour for figures 31-33 .....	33
Figure 31 Top-down pressure contour of base Ahmed at the top surface .....	33
Figure 32 Top-Down pressure contour of Design 1 at the top surface .....	34
Figure 33 Top-down pressure contour of design 2 at top surface.....	34
Figure 34 Top-down view of base Ahmed streamline velocity .....	34
Figure 35 Top-down view of Design 1 streamline velocity .....	35
Figure 36 Top-down view of Design 2 streamline velocity .....	35
Figure 37 Top-down Turbulence Kinetic Energy of base Ahmed at 0.2m height.....	36
Figure 38 Top-down Turbulence Kinetic Energy of Design 1 at 0.2m height .....	37
Figure 39 Top-down Turbulence Kinetic Energy of Design 2 at 0.2m height .....	37
Figure 40 TKE plane location for figures 41-43.....	38
Figure 41 Turbulence Kinetic Energy at -2m behind the base Ahmed model.....	38
Figure 42 Turbulence Kinetic Energy at -2m behind Design 1 .....	39
Figure 43 Turbulence Kinetic Energy at -2m behind Design 2 .....	39
Figure 44 Design 1 inlet Velocity streamlines.....	40
Figure 45 Design 1 outlet velocity streamlines.....	40
Figure 46 Design 2 outlet velocity streamlines.....	41



## Nomenclature

DES	Detached Eddy Simulation
RANS	Reynolds Averaged Navier Stokes
LES	Large Eddy Simulation
IDDES	Improved Detached Eddy Simulation
WMLES	Wall Modeling in Large Eddy Simulation
CFD	Computational Fluid Dynamics
BOI	Body of Influence
CAD	Computer Aided Design
SRS	Scale Resolving Simulations
BL	Boundary Layer
POD	Proper Orthogonal Decomposition
TKE	Turbulence Kinetic Energy

## Chapter I

### Introduction

The Thesis of this research is to investigate the feasibility of wake region manipulation using a fully passive air injection method that will utilize upstream flow and inject it into the wake region of a moving vehicle. Being able to understand and manipulate the wake region of a moving vehicle is especially important, as the wake region of a vehicle moving at 90 km/h accounts for 70% of the aerodynamic drag (Hanfeng & Menxia, 2012). Drag force  $F_d$  is dependent on drag coefficient  $C_d$ , the frontal area  $A$ , and is the density of the fluid  $\rho$ , where those variables remain constant. The most important aspect is the velocity of the vehicle  $V^2$ , an exponential growth. A reduction in drag will not only increase fuel efficiency, but less of the engines power will go to overcoming drag which in turn will have better overall performance (Sovran, H. 1993). This will allow car manufacturers to produce vehicles with smaller engines that will perform much better, reducing their product cost but will also change the racing industry, as faster speeds could be achieved.

$$F_d = \frac{1}{2} C_d \rho V^2 A \quad (1)$$

Where:

$F_d$  = Drag force

$A$  = Cross sectional area

$V$  = Velocity of object

$\rho$  = Density of the fluid

Drag is composed of 2 components, pressure drag, and friction drag. Friction drag is the friction between the surface of the body and the fluid, while pressure drag is related to the cross-sectional area of the body and is important for separated flows. When a body is streamlined, it is said that it is being dominated by friction drag. When the body is dominated by pressure drag, it is called a bluff body (Princeton, 2022),( Thakur et al, 2017).

Past studies have found that pressure drag can be reduced with various methods including active air jets, surface manipulation, passive air control, physical deflectors (Kral. L 2010; B.F. Zang et al, 2018; Brunn, A & Nitsche, W; Bruneau C. et al, 2008; Fourrie, G. et al 2010), and even a combination of passive and active flow control (Bruneau C. Et al, 2009). The passive method proposed in this paper will draw clean air from the front of the vehicle above the windshield as the mass flow rate of air is the highest at that point (Haziqah, Nur & Sukri et al, 2017) in order to carry more energy into the wake region. Passive Flow control has been revisited by automotive companies multiple times over the decades while they attempt to overcome energy balance in order to have an effective result (Burk, A 2014). All methods that have resulted in a significant drag reduction have been rejected by car manufactures as they do not meet visual standards, have power consumption, occupy a significant amount of space, and require instrumentation to control and measure the variables.

The wake region is almost entirely comprised of unpredictable high energy turbulence, making it difficult to accurately resolve as higher computing power is required than available today. To effectively manipulate and/or control the wake region, the passive air needs to carry enough energy to overcome and overpower the energy in the wake region, or the targeted area, in order to significantly reduce drag. In contrast to passive methods using active air jets have provided better results, as the outlet velocity can be controlled and be set to a much higher velocity than the moving air around the vehicle, which provides much higher energy in the jet

output (Kral, L. D. (2000). As previously mentioned, active methods have proven to be effective but there are attributes that cause them to not qualify for everyday vehicle application. A fully passive method will allow implementation on everyday vehicles, as no extra equipment will be needed and no maintenance will be required, and the effectiveness of the design will increase as the speed of the vehicle increases.

As turbulence requires high computational power, fluids engineers have utilized the Navier Stokes equations to create different turbulence models that we can use to resolve turbulence as best allowed with our current knowledge and computational power. In the past, the standard  $k-\omega$  and  $K-\epsilon$  SST turbulence models have been widely used as they provide decent results over a wide range of flows (Shaharuddin, 2017; Chung & Chung, 2002). When modeling turbulence in the wake region, the Detached Eddy Simulation (DES) model was used as it combines Reynolds Averaged Navier Stokes (RANS) and Large Eddy Simulation (LES), which is why it is also known as hybrid RANS/LES. This model allowed more accurate results than using RANS but is also less computationally heavy than LES (P. Spalart, Jou, Strelets, & Allmaras, 1997). Later on in 2006 P.R Spalart et al. (2006) introduced Delayed Detached Eddy Simulation DDES as DES would produce results that were not accurate when the cell sizing was smaller than the boundary layer. This was due to the fact that it would switch to LES early and try to resolve the flow where the mesh was not fine enough for LES to fully resolve (Kaloki, N. 2020). Shur et al. (2008) introduced Improved Delayed Detached Eddy Simulation (IDDES) that blends DDES and Wall Modeling in Large Eddy Simulation (WMLES). This allows for more accurate results with less computational power requirements but is heavily dependent on wall modeling. Davidson (2009) stated that to have accurate results the following criteria needed to be met;  $Dx^+ \approx 100$ ,  $Dy^+ \approx 1$ , and  $Dz^+ \approx 30$ . This is achieved by doing a parametric study and adjusting the mesh settings, more specifically first layer height, until the parameters are satisfied.

Within the last decade, the IDDES turbulence model has been found to be more accurate when it comes to wake modeling where results were obtained with a 0.85% difference with experimental values (Kalokli. N, 2021). Cho et al (2018) also found that IDDES produced drag coefficients more consistent and accurate with experimental models, which is why this “new” turbulence model is now being used to study the wake region and drag.

Most experimental turbulence CFD test utilized the Ahmed bluff body to perform their comparison between computational and experimental wind tunnel data so the results could be easily comparable, as it would function as a controlled variable. Ahmed (1984) proposed this generic bluff body used to study flow over a moving vehicle and to study the wake region, as it is dominated by pressure drag, making it ideal for preliminary wake region studies. This model is known as the Ahmed Body, and it is being used to this day for wake region analysis. The same body is used to observe the effects of a passive air injection into the wake region in efforts to reduce pressure drag. As the Ahmed body will be used for this preliminary study it is important to understand the relationship between the DrivAer Model and the Ahmed body. Figure 1 below shows the key locations on the DrivAer model and their equivalent locations on the Ahmed body. As the Ahmed body is a Bluff body, there is no B-pillar, and only the A-pillar and C-pillar locations are identified.

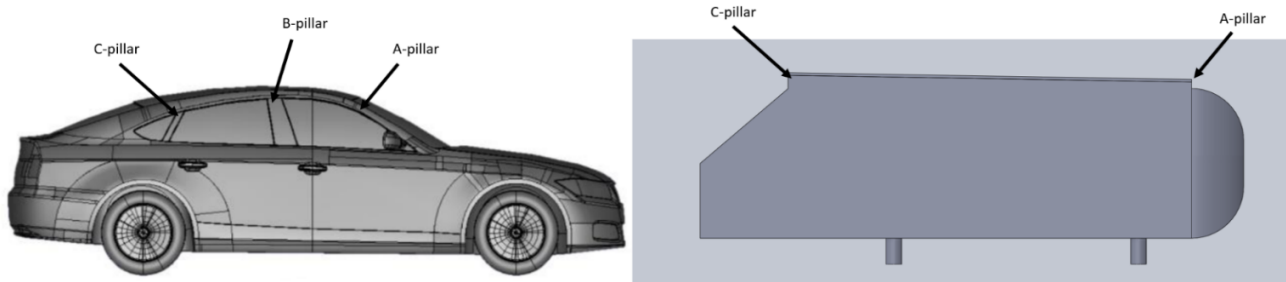


*Figure 1 DrivAer model and Ahmed body pillar locations*

Whilst many have tried to manipulate the wake region by injecting air into the wake region to reduce or delay flow separation above the rear window, Rossitto G et al (2016) found that by reducing the C-pillar vortex strength there was a reduction in drag. The study also found that the C-pillar vortex would penetrate the slanted surface towards the center line, shown in figure 2. This was found to reduce the vertical base pressure and in turn increase drag and have an impact on the overall behavior of the wake region. This study agrees with the previous findings of vortex shredding in the wake region conducted by, Berger & Wille (1972), Lin & Pao (1979), Bearman (1984), Oertel (1990), Griffin & Hall (1991), Coutanceau & Defaye (1991), and Williamson (1996, 2004).

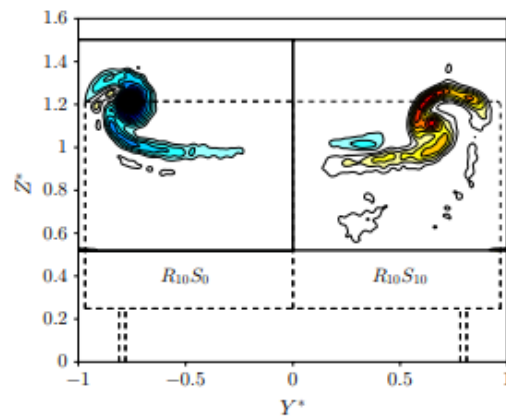


Figure 2 C-pillar vortex distribution, (Rositto G, et al. 2016)

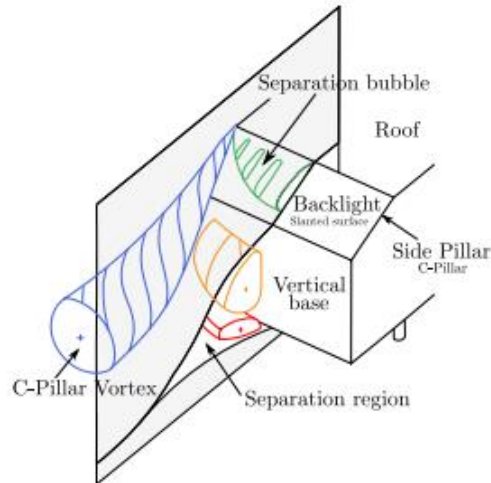


Figure 3 wake region breakdown, (Rositto G, et al. 2016)

The purpose of this research is to investigate the feasibility of passive clean air injection into the wake region on moving ground vehicles. The drag force will be recorded which then will be translated to the Drag coefficient and compared between two concept designs and the base Ahmed model to see the effect that passive clean air injection has on the vortices generated by the C-Pillar shown in figure 3, in efforts to reduce pressure drag caused by the wake region. By setting the location of the outlets close to the C-pillar vortex, there is a greater probability that the behavior would change downstream. By pushing the C-pillar vortex further away from the

body and/or reducing its strength the separation bubble and the vertical base separation bubble will increase in pressure, thus reducing the pressure drag of the overall vehicle (Rossito G, et al. 2016). This study will attempt to draw clean air from the front of the vehicle, and by utilizing conservation of mass and a venturi shaped design, inject the air into the wake region. Bernoulli's principal has been utilized in the automotive industry by implementing an underbody diffuser that allows the pressure difference and the higher velocity air to create more downforce by creating lower pressures under the vehicles and to reduce drag by creating a smaller wake region (Huminic, A & Huminic, G 2020). A similar concept will be applied in this study as the upstream flow will have less energy than the turbulence in the wake region, which will assist in drawing the clean air into the wake region. By understanding the wake region and implementing a simple passive control method, not only will the automotive industry change, but this design could be implemented on various objects that either travel through fluid or have fluid flow around them.

## **Chapter II**

### **Literature Review**

No matter the methods, all aerodynamic analysis stems from the Navier Stokes equations. The Navier Stokes equation consists of three main equations: energy conservation, momentum conservation, and mass conservation. In this study, the flow is in the lower regions of subsonic flow, thus any compressibility effects that would affect the Navier Stokes equations are neglected. This leaves only conservation of mass and conservation of momentum which are shown below with equations 2 and 3 respectfully.

$$\nabla \cdot \vec{V} = 0 \quad (2)$$

$$\rho \left( \frac{\partial \vec{V}}{\partial t} + \vec{V} \cdot \nabla \vec{V} \right) = -\nabla p + \mu \nabla^2 \vec{V} \quad (3)$$

Where:

$\vec{V}$  = velocity vector

$\rho$  = density

t = time

$\mu$  = dynamic viscosity

p = pressure

All CFD calculations revolve around solving the Navier Stokes equations, and Scale Resolving Simulations (SRS) which resolve part of the turbulence in some locations (Gritskevich. M, et al, 2012). The major differences are in the turbulence model used that determine how the boundary layer (BL) is being resolved and to what extent the turbulence is being calculated. Turbulence is a very unpredictable phenomenon where we can't accurately solve the Navier Stokes equations due to a lack of computational power and understanding of turbulence. This has led to the creation of several turbulence models which further increase the accuracy of the calculations but come at a cost of computational power.

### **Past methods of wake manipulation**

From the time that Tokumaru & Dimotakis (1991) found an experimental drag reduction of 80% using active methods, many have explored this topic with various approaches such as oscillations of a bluff body, inflow oscillation (Konstantinidis et al. 2005, Nehari et al. 2004), steady blowing/suction (Arcas & Redekopp 2004, Delaunay & Kaiktsis 2001, Leu & Ho 2000, Lin et al. 1995, Sevilla & Martínez-Bazán 2004, Yao & Sandham 2002), time-periodic blowing/suction (Fujisawa et al. 2004, Jeon et al. 2004, Lin et al. 1995, Williams et al. 1992), rotary (Baek & Sung 1998; Choi et al. 2002; Dennis et al. 2000; Filler et al. 1991; Poncet 2002, 2004; Shiels & Leonard 2001; Tokumaru & Dimotakis 1991), with all resulting to the same conclusion, the efficiency of the systems was not high enough to implement on real situations (Choi, H. et al. 2008).

Over the years this topic has been revisited repeatedly, with one of the most promising solutions being active air jets, which showed a drag reduction of up to 29% (B.F. Zang et al). This method has been investigated by many since. Barsotti, L. (2015) found that active jets with a velocity of 10.2 m/s achieved a drag reduction of 22% for an Ahmed Body of a slant angle of 24 deg. In his study Proper Orthogonal Decomposition (POD) was used to visualize the turbulent coherent structures in the near wake of the Ahmed body and using IDDES turbulence model.

The more effective method of passive drag reduction was surface manipulation, where the surface of the roof was porous on key locations and a drag reduction of 22% was found (Bruneau C. Et al, 2010). The study agreed with findings that Bruneau C. Et al (2008) found using a 2D Ahmed body. Where porous material was applied on the surface in efforts to reduce drag. Additionally, Suzuki, Y (1999) found a drag reduction of up to 50% was found, when using artificially rough surfaces, while a variety of different surface manipulations such as splitter plates (Anderson & Szewczyk, 1997; Hwang et al., 2003; Kwon & Choi, 1996; Ozono, 1999), and longitudinal groves (Lim & Lee, 2002).

The least effective method that has been studied is the implementation of physical deflectors to delay the generation of counter rotating vortices (Fourrie, G. et al, 2011). Hanfeng, W et al. (2016) found that in some cases physical deflectors would increase drag if they were too large and mounted on the side. In contrast, deflectors mounted over the rear window of a vehicle could achieve drag reduction of up to 11.8% in comparison to 7.6% of the side mounted deflectors. In both cases, a reduction in the C-pillar vortex was noticed that led to the pressure drag reductions. This suggests that the manipulation of the C-pillar vortex could drastically affect the entire wake region.

### **Venturi concept**

A venturi, shown in figure 4, is used to drop the pressure in the throat and is typically used to draw fluid in that region as the pressure difference will act as a vacuum, while then gradually introducing the flow back into ambient conditions as to avoid flow separation and turbulence creation. By dropping the pressure in the throat of the venturi the velocity of the fluid increases. This is shown in Bernoulli's Equation below. Since fluid density, acceleration due to gravity, and height remain constant, they can be neglected. This results in only pressure and velocity being accounted for in equation 4 for this experiment. This creates a relationship between the inlet and outlet that will assist in drawing air from the inlet and increasing the pressure in the wake region, as the equation must remain true.

$$P_1 + \frac{1}{2}\rho v_1^2 + \rho g h_1 = P_2 + \frac{1}{2}\rho v_2^2 + \rho g h_2 \quad (4)$$

Where:

$P_1$  = Pressure on side 1

$\rho$  = Density of the fluid

$v_1$  = Velocity on side 1

$g$  = acceleration due to gravity

$h_1$  = height on side 1

$P_2$  = pressure on side 2

$v_2$  = velocity on side 2

$h_2$  = height on side 2

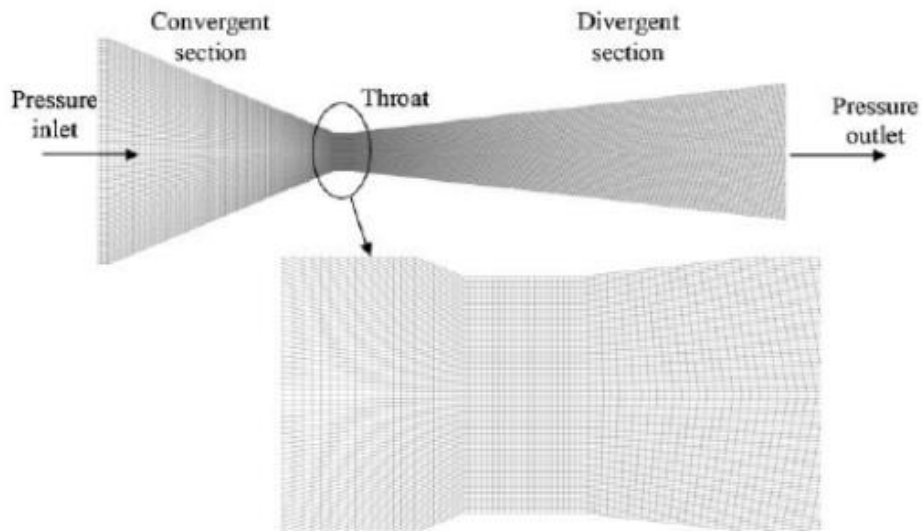


Figure 4 Venturi design (Bashir A. 2011)

The venturi concept is applied to vehicle underbodies and manipulated with the implementation of an underbody diffuser. As mentioned previously, as the velocity increases, the pressure on the same side of the equation must decrease to keep the equation true. This creates a suction on the underbody of the vehicle, increasing the downforce. The downside of a venturi is

that right after the throat there is a lot of energy loss due to turbulence and a big pressure drop (Bashir. A, et al., 2011). One phenomenon that occurs at the throat of the venturi is cavitation, which are a release of large magnitudes of energy over a small location that result in high energy densities (Young, 1989; Mason, 1992; Leighton, 1994). These high energy density areas are at the throat of the venturi.

## **Chapter III**

### **Methodology**

This research was conducted using Solidworks, Ansys 2022 Workbench with Fluent meshing, SpaceClaim and CFDPost, starting with Solidworks and the CAD design of the Ahmed body, which was then imported into SpaceClaim to create the enclosure, BOI and indicate the different regions/boundary conditions. Once all boundary conditions are identified, and the enclosure is set, the file was imported into Ansys Fluent mesher to create the mesh and make any necessary adjustments to the mesh so certain criteria are met by adjusting the number of cells that fall within the boundary layer by conducting a mesh independent study. Once the mesh was created the boundary condition and environmental values were set, and the simulation was run. In order to have a visual representation of the flow behavior and to collect computational values, CFDPost was used. This allowed the use of Streamline, Pressure contours, Turbulence Kinetic Energy visualizations, as well as force calculations.

#### **Passive air injection solution**

Shaharuddin (2017) shows that the highest air flow occurs right above the front windshield of the car which also applies to the Ahmed body as seen in figure 5 below. By implementing an inlet at the front of the roof, in the location shown in figure 5 where the flow is at its peak velocity, high

energy flow will be captured and travel through the interior of the roof all the way to the top of the rear windshield in efforts to be injected in the wake region.

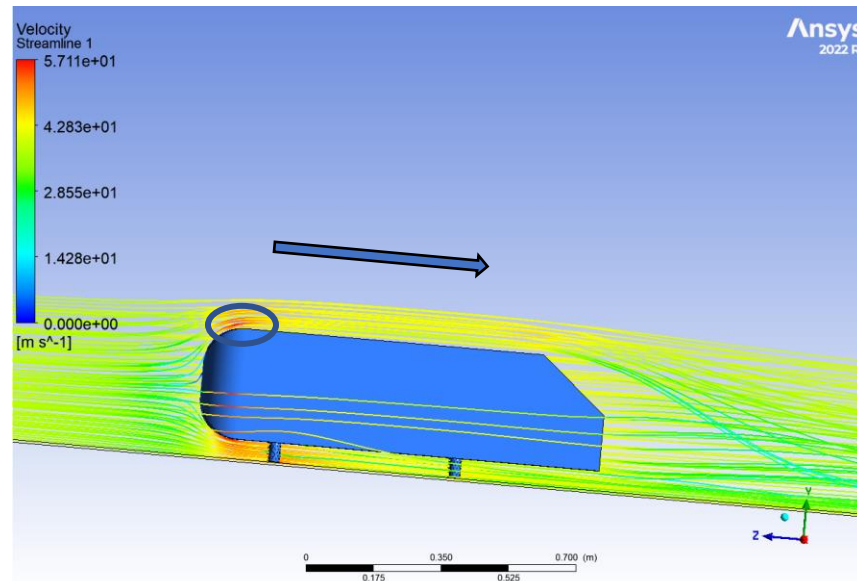


Figure 5 Inlet location

By injecting “clean” air at targeted locations in the wake region, the overall behavior and pressure will be affected. This design will be focusing on manipulating the C-pillar Vortex in by reducing the pressure in the wake region in efforts to move the C-pillar vortex further away from the center line, allowing for a more linear pressure equalization in the wake region and in turn a lower pressure difference which would result in less pressure drag.

As mentioned earlier in efforts to inject high energy flow, the pathway that the air will follow will utilize a venturi shape, with an angle increase of 1 degree to maintain the higher flow speed from the inlet while reducing the outlet width, while also ensuring there will be no flow separation. The reduction of outlet width is necessary as that it is how the injection can occur in specific locations. Being able to maintain a high energy injection dictates how impactful it will be. The higher the energy in combination with higher volume of air will be able to affect the wake region further. In efforts to reduce drastic pressure changes within the roof of the vehicle,

the conservation of mass equation shown in equation 5 below was used to calculate the inlet and outlet areas, such that the mass flow rate in, is equal to mass flow rate out.

$$\rho A_1 V_1 = \rho A_2 V_2 \quad (5)$$

Where:

$\rho$  = Air density

A = Area

V = Air velocity

### **CAD setup**

The first part of this research was conducted using the Ahmed body, shown in figure 6 to validate the mesh settings with experimental wind tunnel results. By importing the CAD into Spaceclaim, the enclosure was created using the parameters shown in Table 1 which are up to the user's discretion, if the enclosure is large enough to allow the flow to fully develop downstream and not cause any flow disruptions. If the enclosure is too large it will come with a large computational cost. The values used in this study are considered good practice in the CFD community. A BOI was created that started 1m ahead of the Ahmed model and ran for 10 Body lengths downstream to allow the full development of the wake region. The purpose of the BOI is to create a finer mesh in the specific areas that were being investigated to obtain more accurate results. Once the mesh settings were validated, two designs were tested. Design 1 composed of 1 inlet at the front of the vehicle, and 2 outlets at the rear of the vehicle at each corner with no angle offset. Design 2 implemented Barsottis, L (2015) findings where the optimum angle of active jet injection was 25 degrees.

Table 1 Enclosure Parameters

Table 1 Enclosure parameters		
Width	18*Body width	7020 mm
Trailing Length	18*Body Length	18720 mm
Height	12*Body height	3480 mm
Inlet distance from front of body	5*Body length	5200 mm

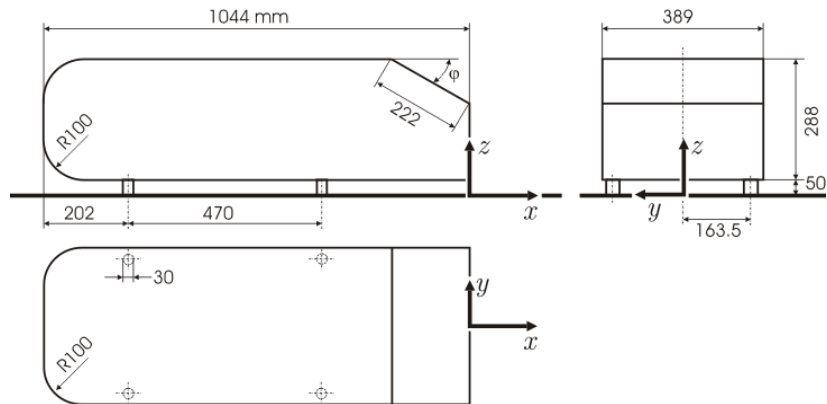


Figure 6 Basic Ahmed Body CAD setup

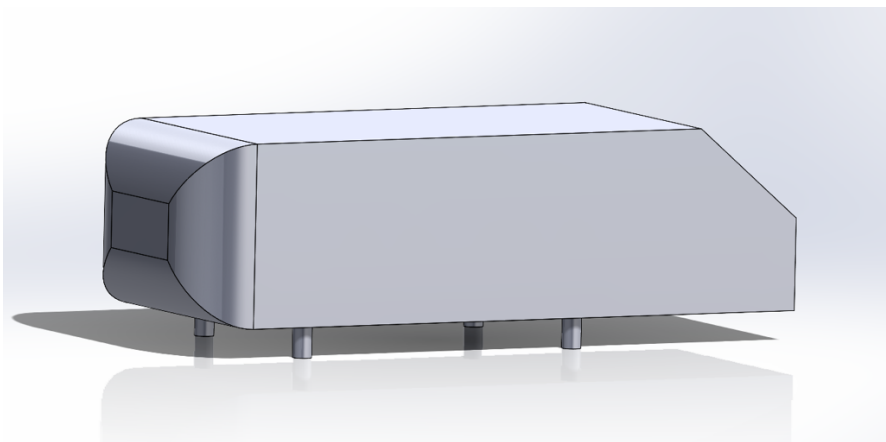


Figure 7 Basic Ahmed body CAD

As show in figure 8 below, the proposed design will be implemented in the roof of the Ahmed body, resulting in a closed roof design. Utilizing a venturi design with a wide inlet, and slowly reducing the path to two narrower but taller outlets the velocity of the inlet air will be maintained and to conservation of mass will be followed as stated previously.

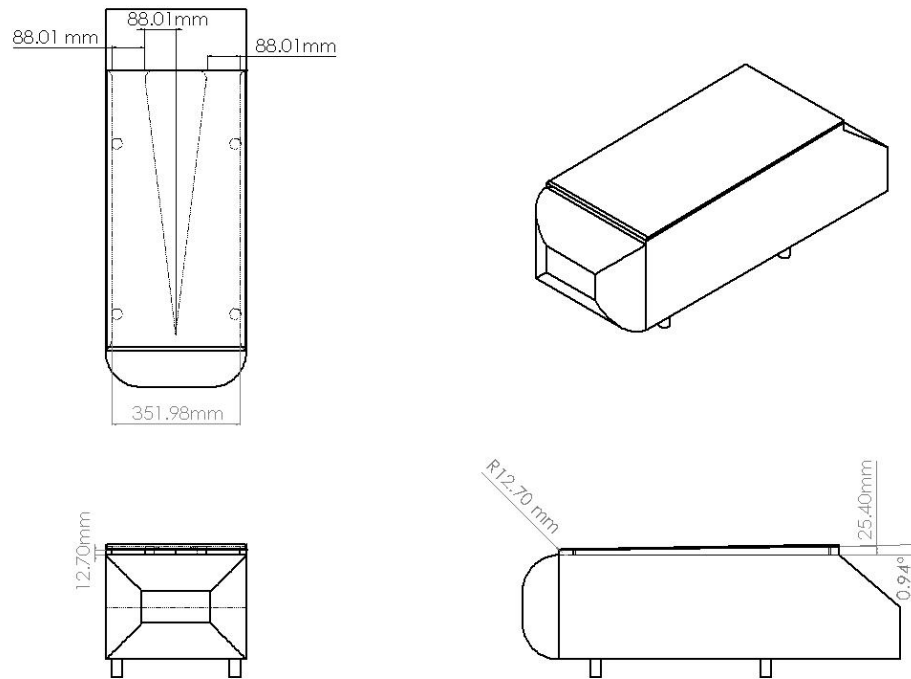


Figure 8 Design 1 design

In figure 9, design 2 is shown, where the implementation of a 25-degree slant is used at the outlets of design 1, utilizing the findings of Barsotti, where the optimum jet angle were 25 degrees for active jets.

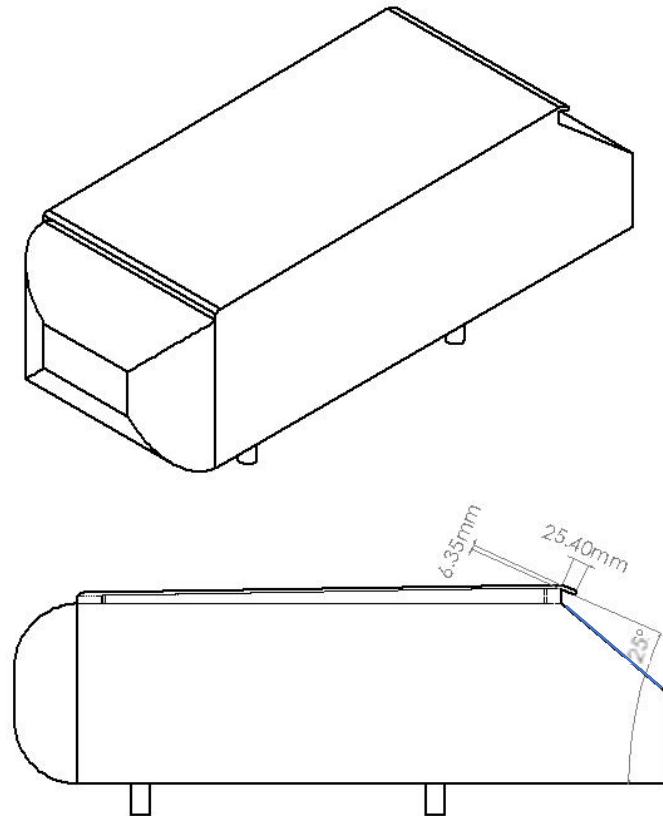


Figure 9 Design 2 implementation

### CFD analysis

Testing the concept will consist winds of 40m/s which translates to approximately 90 mph where the wind tunnel testing took place, as well as 20 m/s which translates to approximately 45mph, where most daily vehicles operate in. All simulations utilized the  $K\omega - SST$  turbulence model for the analysis as they are less computational heavy reducing the run time of the experiment. Meile. W (2014) shows that the  $K\omega - SST$  model was verified in comparison to other models and experimental data and was found to be within an acceptable 5% error range.

Setting up the boundary conditions in Ansys were as follows: Inlet as a velocity inlet, outlet as a pressure outlet, the ground as a moving ground matching the air speed, and the

remaining walls were declared as symmetry as to replicate an open environment. It was found that meshing the entire enclosure and BOI was computationally heavy, and as this research is a preliminary study of the feasibility of a fully passive air injection method a half model for the CFD analysis was used. This meant that once the enclosure and BOI were created in SpaceClaim, they were then cut in half, utilizing half of the Ahmed body. By using the half body, the wake region could have not been resolved fully as the middle wall used symmetry. As discussed earlier, the wake region vortices tend to cross over the midpoint of the vehicle, which could lead to inaccurate results. To ensure that the half model produced accurate results these cases were validated as shown later in this paper and compared to experimental wind tunnel data. All Simulations were run for 22.5 seconds of flow utilizing transient time steps as the state the flow had stabilized and all residuals were steady. Once CFD testing was conducted the case and results files were loaded into CFDPost, where all post processing would be done to get numerical values and visual representations. Within CFDpost the Drag Force was calculated while the cross-sectional area was determined from Fluent as to avoid calculation errors, and a constant air density of  $1.225\text{kg}/\text{m}^3$  were used to calculate the Drag coefficient by using equation 6 below.

$$C_d = \frac{F_d}{\frac{1}{2}\rho V^2 A} \quad (6)$$

Streamlines, Vorticity, Pressure contours, and Turbulent Kinetic Energy (TKE) contours were then created on areas of interest to see the flow behavior before and after the concept design to analyze the C-pillar vortex behavior and observe the pressure changes. Streamlines are a quick and straightforward way to visually understand the flow behavior, while pressure contours can show us more of the effect that the flow has on the body. Turbulent Kinetic Energy contours will help identify the intensity of turbulence in the flow, the higher the TKE value, the

lower the pressure is in that region. The combination of the visualization of the flow, along with the numerical values, we can get a better understanding of the effects of the concept design.

### Mesh independent study

In order to find the optimal mesh settings a mesh independent study was conducted, shown in figure 10 below, using the base Ahmed half model for additional validation and to determine the lowest cell count required to compute accurate results in efforts to reduce computational time.

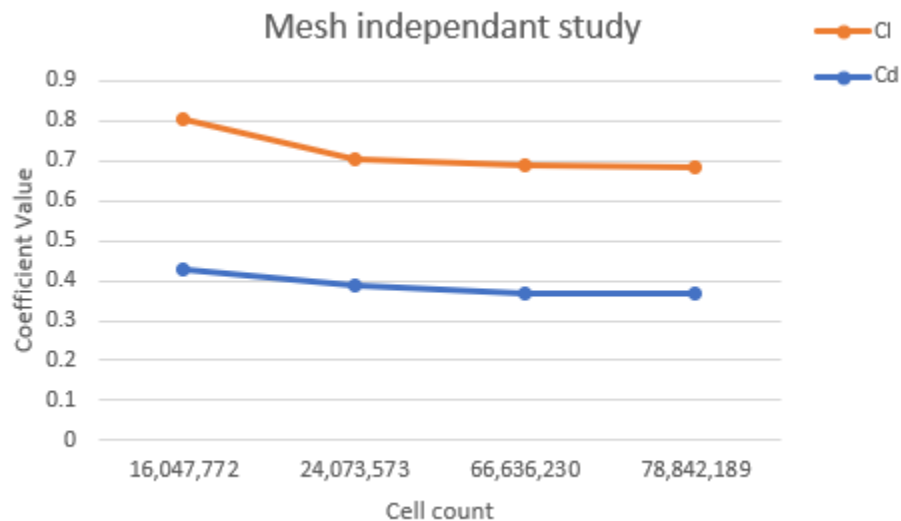


Figure 10 Mesh independent study results

In table 2, each data point is shown as well as the percent difference to the previous data set. As shown in the table below, the mesh settings were adjusted to produce a finer mesh each iteration until a mesh produced 78,842,189 cells was used that resulted in a 0.54% difference to the previous mesh settings. As the increase was not significant, the mesh settings that produced 66,636,230 cells were used, as they provided results that were within an acceptable error range of the experimental data, and the computational requirements were lower.

Table 2 Mesh Independent Study

Table 2 Mesh independent Study			
Cell count	$C_l$	$C_d$	$C_d$ % Difference
16,047,772	0.43	0.3758	N/A
24,073,573	0.39	0.3158	9.76
66,636,230	0.37	0.3167	5.26
78,842,189	0.36	0.32	0.54

Once the Mesh settings were determined and the mesh independent study was complete, the final mesh of the half enclosure and BOI were created where the BOI had a finer mesh than the rest of the enclosure. This allowed the turbulence equations to be more accurately resolved, which allowed more accurate visual models and calculations to be generated in the wake region and around the moving vehicle.

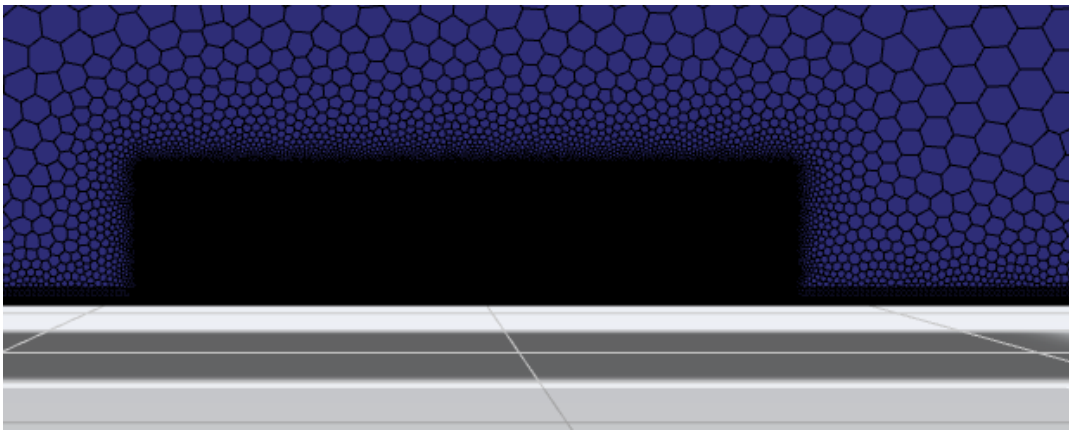


Figure 11 Enclosure and BOI Mesh

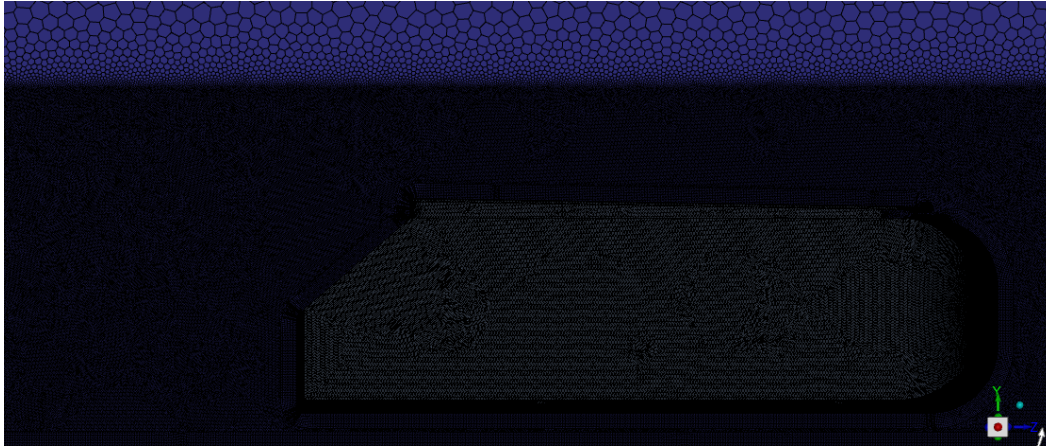


Figure 12 Close up of BOI and body surface mesh

## Chapter IV

### Discussion, Conclusion, and Recommendations

Table 3 CFD Results

Model	$C_l$	$C_d$ at 40 m/s	$C_d$ at 20 m/s	$C_d$ Percent difference from experimental data at 40 m/s	$C_d$ Percent difference from base sim data at 40 m/s
Base Ahmed model	0.37	0.3167	0.3169	+ 3.6%	N/A
Design 1	0.23	0.2822	0.2883	- 5.78%	11.52%
Design 2	0.24	0.2849	0.2895	- 4.83%	10.57%

To better understand the results in table 3 and the effects of the passive air injection, the pressure contours, streamlines and TKE were applied to visualize the results with all values being localized on the planes displayed as to better identify the numerical values and have a more distinct visual difference. As discussed earlier drag has an exponential growth as velocity increases, for that reason and the insignificant difference of coefficients between 20m/s and 40m/s, the results of 40m/s are used to better visualize the wake region.

Figures 13,14, and 15 show the pressures at the midplane of the base Ahmed body, Design 1, and Design 2 respectively. In figure 13 a low-pressure pocket in wake region is shown

right at the end of vehicle with an approximate pressure of  $-481.7$  Pa, whereas in figure 14 and 15 that low pressure region is gone, and the overall pressure in the same region has been increased to an approximate  $-428.3$  Pa and is more evenly distributed. In figure 15 we can see that the pressure at the end of the vehicle is approximately similar to Design 1.

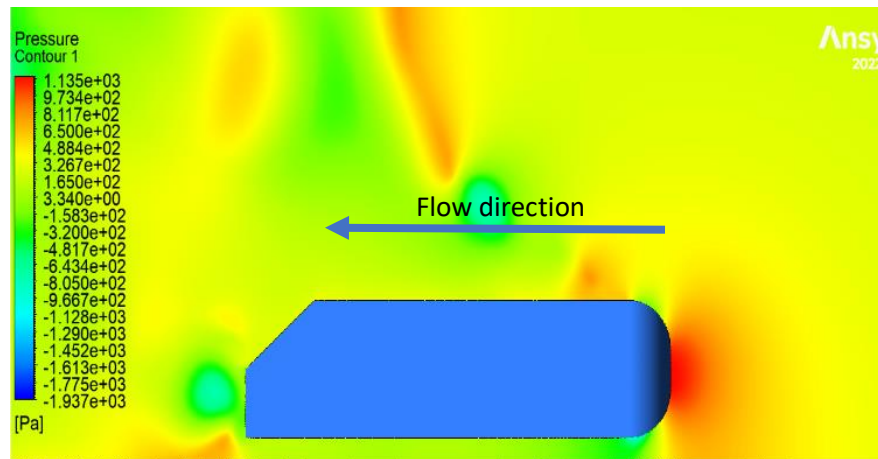


Figure 13 Pressure Contour of base model side profile

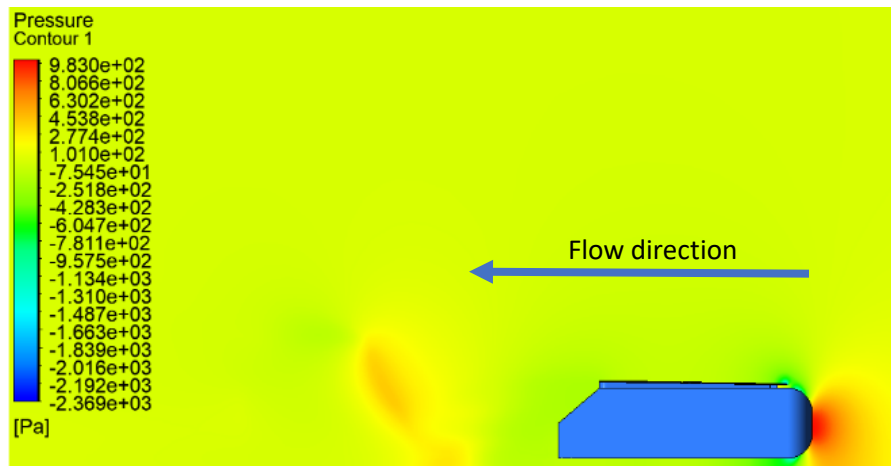


Figure 14 Pressure Contour of design 1 side profile

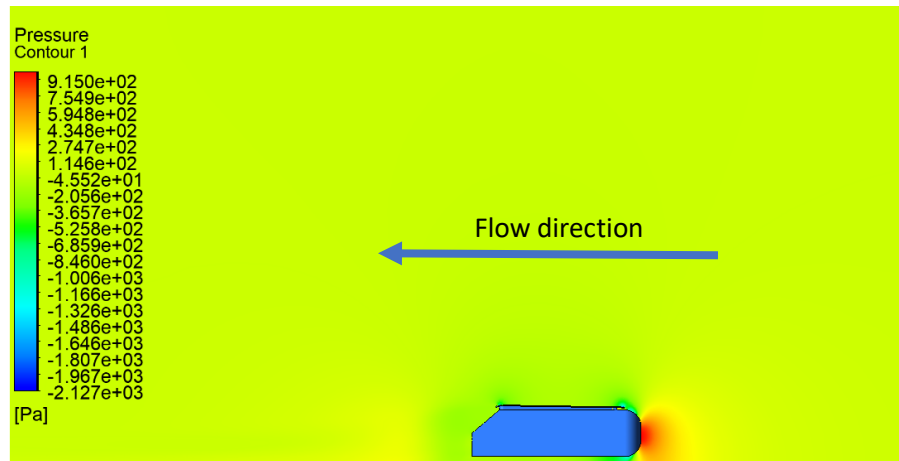


Figure 15 Pressure contour of design 2 side profile

This can be further noticed in figures 17,18, and 19 that show the pressures at the rear of the models, shown in figure 16. In figure 17 a lower pressure is shown at the rear of the base Ahmed model with drastic pressure variations, while in figure 18, higher pressures were achieved overall, as well as being more uniform than the base Ahmed model. Additionally, in figure 19 the formation of the C-pillar vortex is noticed, where the C-pillar vortex has not yet formed on the base model and Design 1. Moving further away from the vehicle, the C-pillar vortices are clearly shown with low pressure areas.

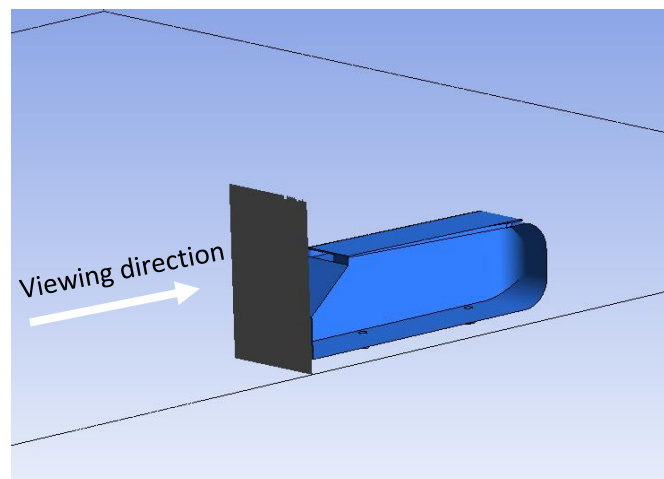


Figure 16 Location of pressure contour for figures 17-19

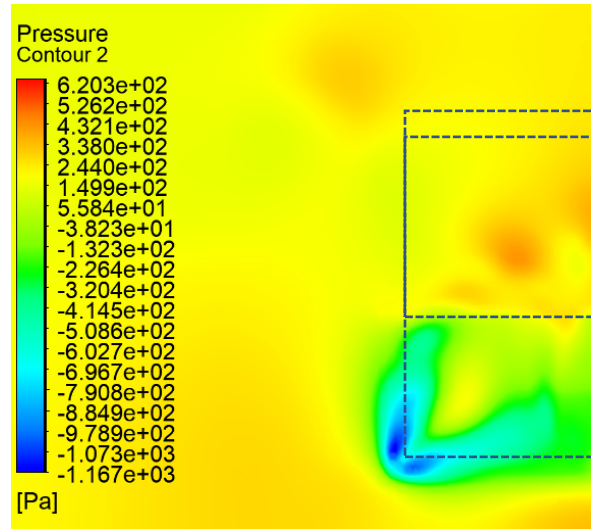


Figure 17 Pressure Contour at rear of base Ahmed model

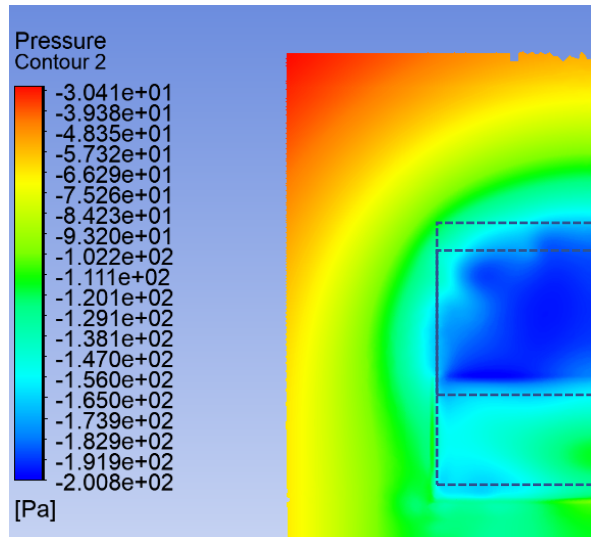


Figure 18 Pressure Contour at the rear of Design 1

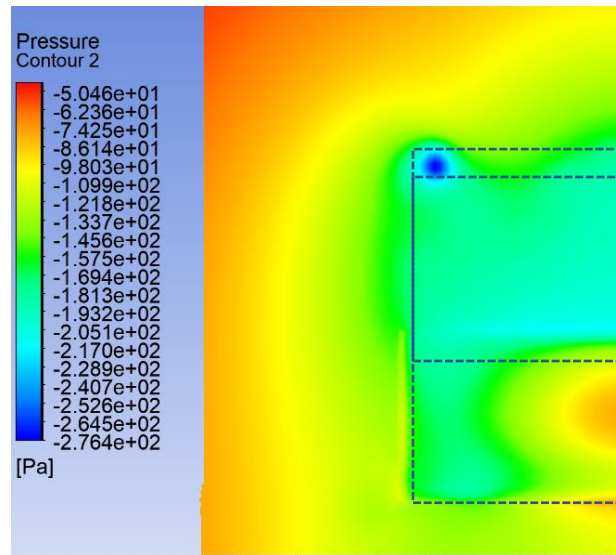


Figure 19 Pressure contour at the rear of Design 2

Similarly, to figures 17,18, and 19 lower pressures are noticed in figure 21, with the C-pillar vortex being noticeably weaker and smaller with the implementation of Design 1 when compared to the base model in figure 21. On figure 23 it is noticed that the C-pillar vortex is weaker as well as higher pressures are distributed over all in the wake region of Design 2. Additionally in figure 22, even higher pressures are noticed above the moving ground with the implementation of Design 1

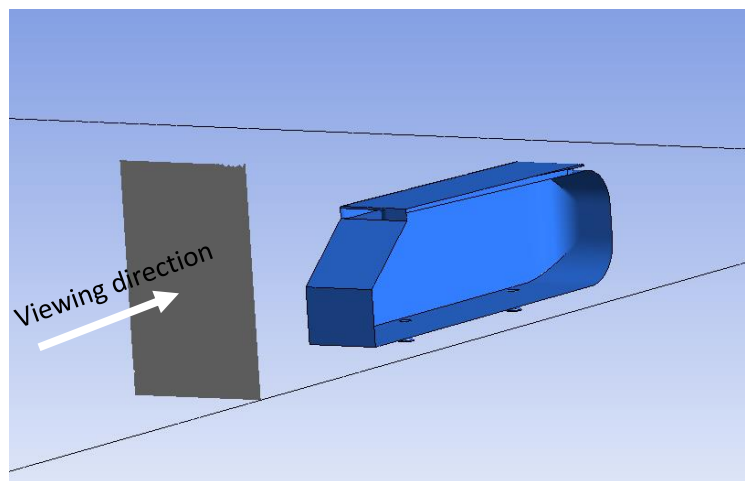


Figure 20 Location of pressure contour for figures 21-23

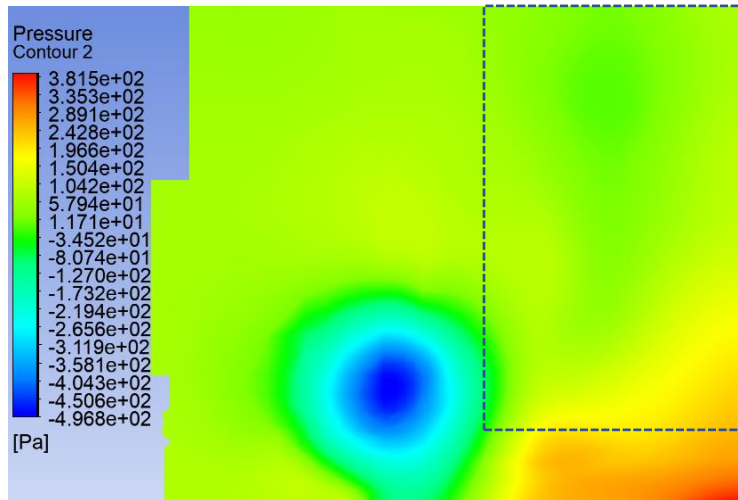


Figure 21 Pressure Contour 0.5m behind the base Ahmed model

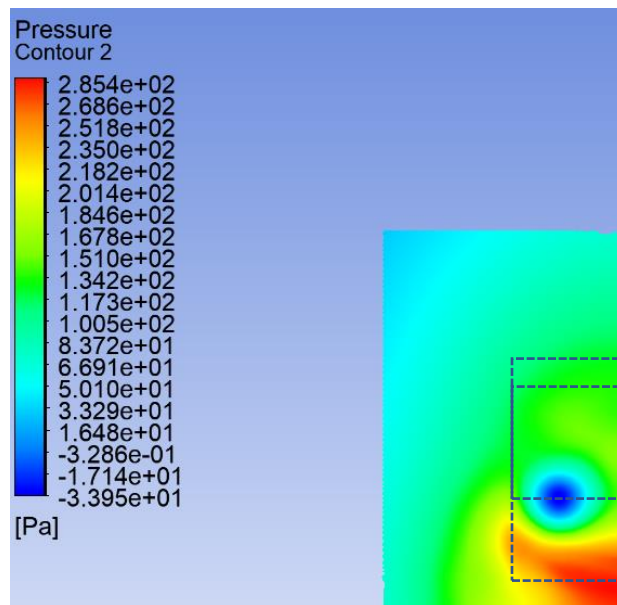


Figure 22 Pressure Contour 0.5m behind Design 1

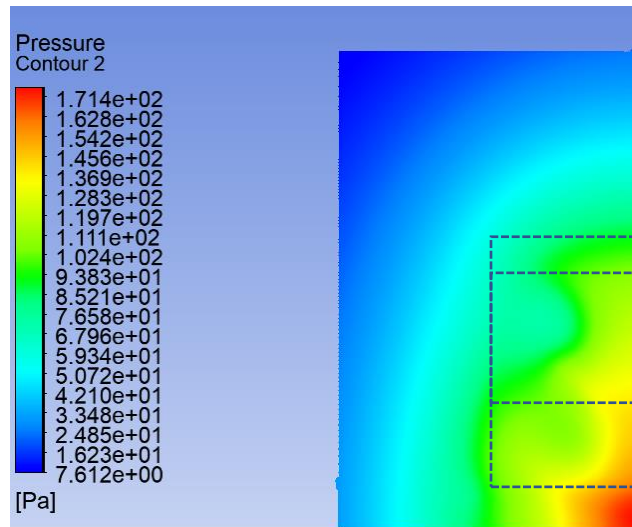


Figure 23 Pressure contour 0.5m behind Design 2

Figures 24 through 33 show the pressures from a top-down view at various heights of the vehicles. In all figures a similar pattern is observed: a more pressure uniform wake region with the implementation of the passive air injection with both Design 1 and 2, where Design 2 had slightly lower pressures achieved when compared to Design 1 by 24.45% in the wake region

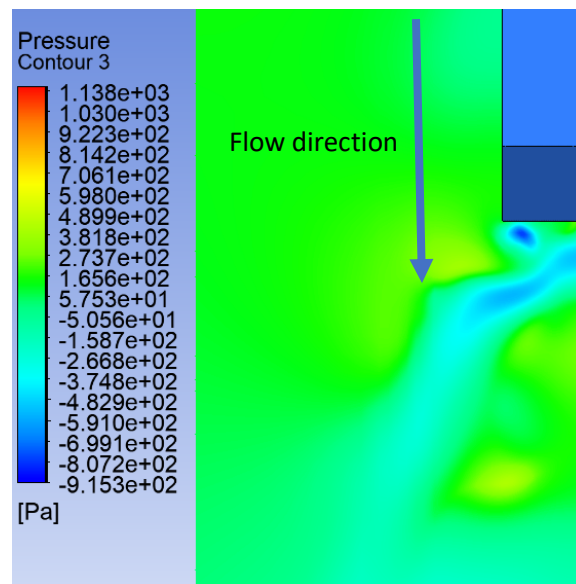


Figure 24 Top-down pressure contour of Ahmed model at half height

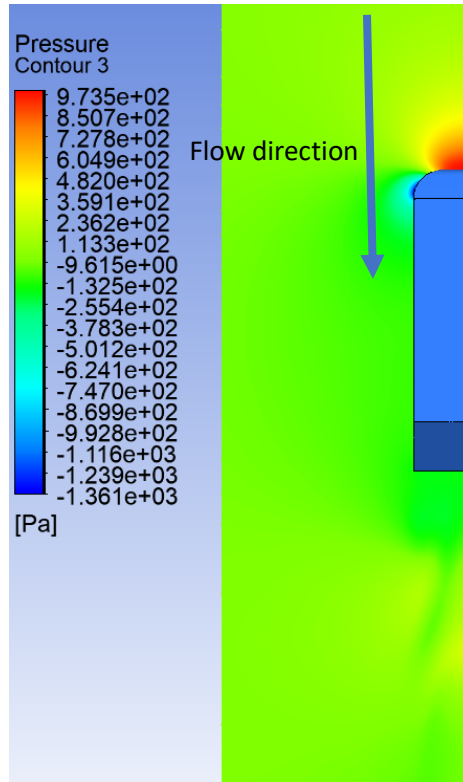


Figure 25 Top-down pressure contour of Design 1 at half height

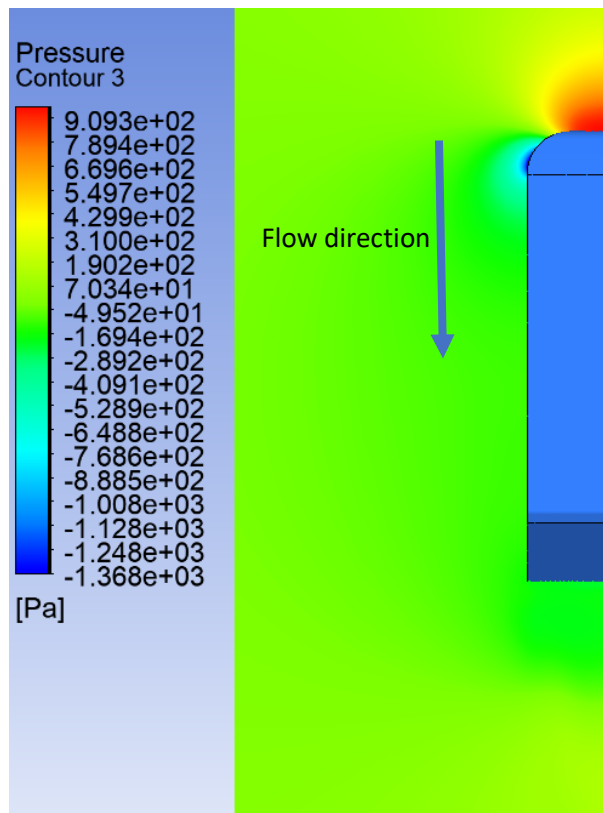


Figure 26 Top-down pressure contour of design 2 at half height

Figures 27 through 29, show a top-down view at 0.2m height, where the findings agree with previous results of a more uniform pressure distribution with the implementation of passive air injection. Design 1 had higher pressures in the wake region of -182 Pa, where the wake region of Design 2 had a pressure of -205 Pa which is an 11.89% difference.

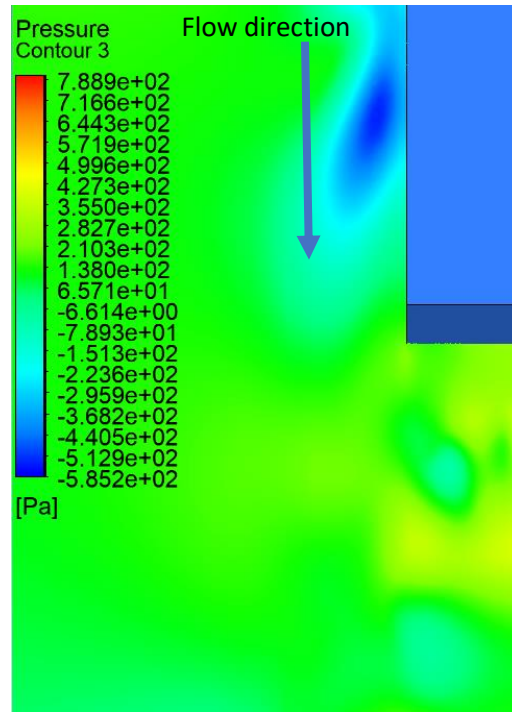


Figure 27 Top-down pressure contour of base Ahmed model at 0.2m height

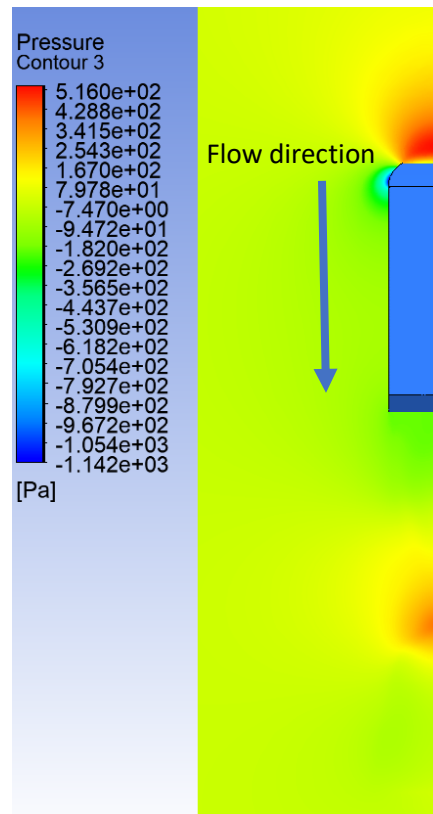


Figure 28 Top-down pressure contour of design 1 at 0.2m height

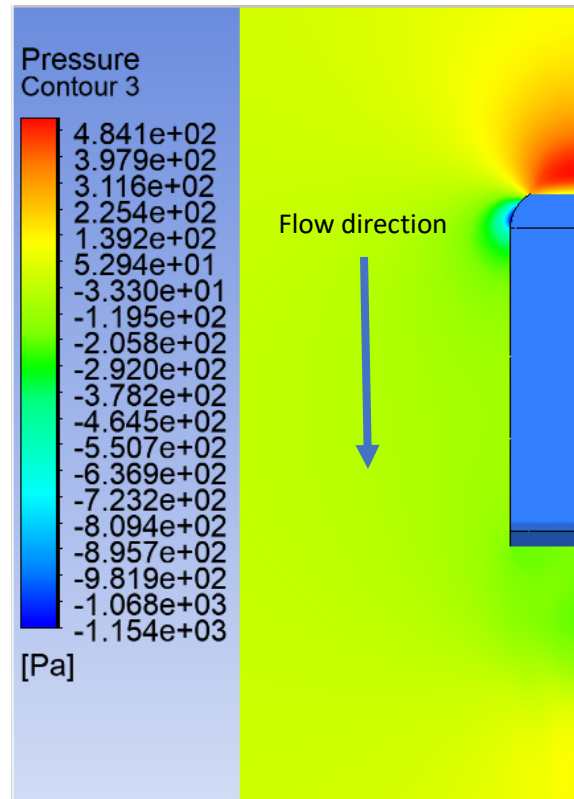


Figure 29 Top-down pressure contour of design 2 at 0.2m height

Figures 31-33 show the top-down pressures of the top surface level of each model, on the plane shown in figure 30 below. Figures 32 and 33 agree with all previous results, where there is a more uniform pressure distribution as well as lower overall pressures with the implementation of passive air injection. Additionally, the C-pillar vortex formation is shown in figure 31 with the base Ahmed model, whereas in both figures 32 and 33 the C-pillar vortex is not visible at this location. The implementation of Design 2 a low-pressure region can be noticed right above the outlets, this is due to the sudden 25 degree drop of the surface, which created flow separation as shown in figure 46. Comparing Design 1 to Design 2, it is noticed that the wake region of Design 1 has a pressure of approximately, -20.95 Pa, and Design 2 has a pressure of -79.17 Pa, which is a 116% difference, while the pressure in the wake region of the base Ahmed model is approximately -205.8Pa which is greater by a factor of 10 when compared to Design 1.

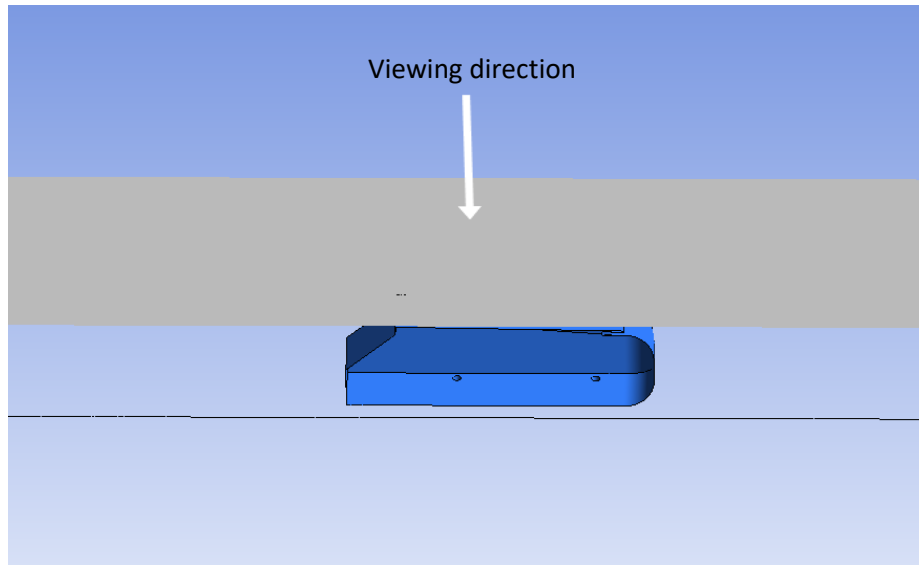


Figure 30 location of pressure contour for figures 31-33

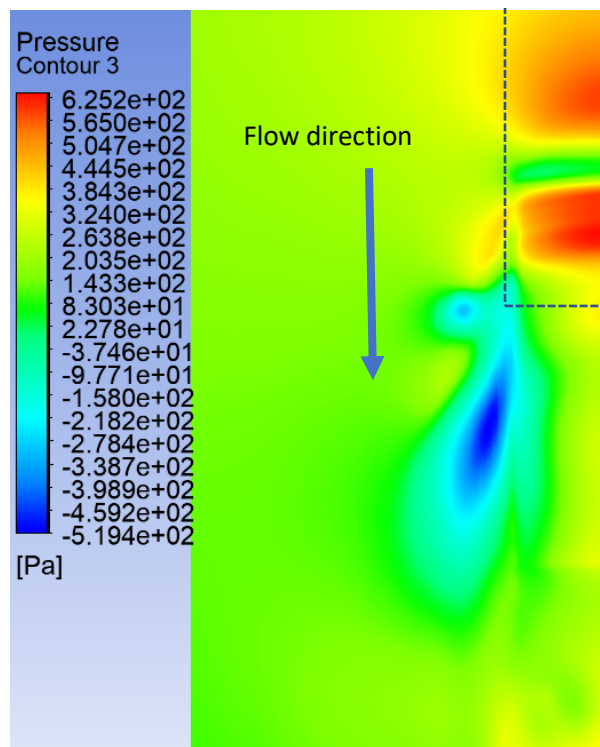


Figure 31 Top-down pressure contour of base Ahmed at the top surface

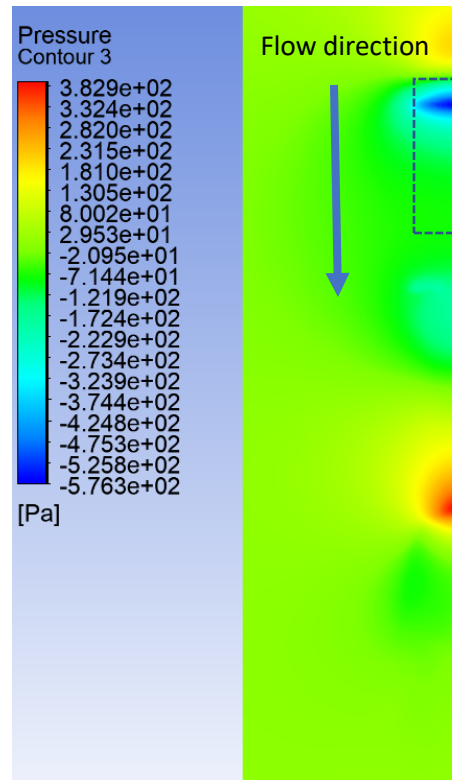


Figure 32 Top-Down pressure contour of Design 1 at the top surface

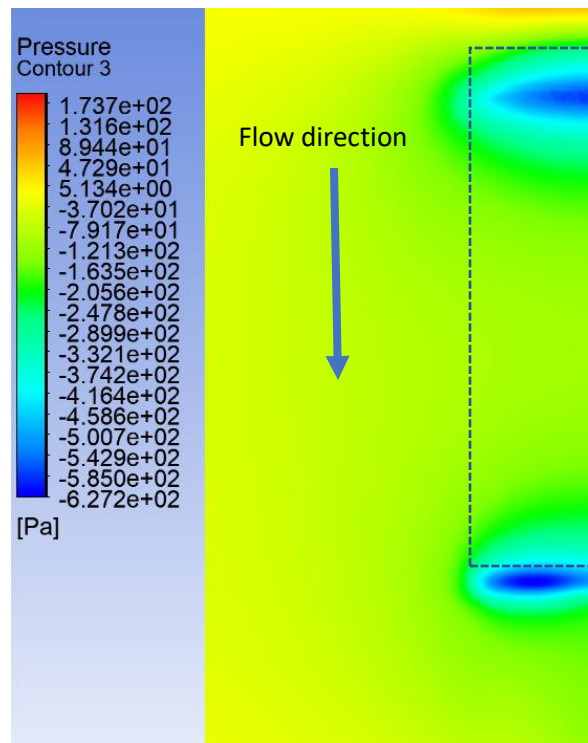


Figure 33 Top-down pressure contour of design 2 at top surface

Applying streamlines upstream, a better visual of the fluid flow could be determined, this is shown in figures 34,35 and 36, where figure 34 shows the flow over the base Ahmed model. In this figure it is shown that the fluid velocity is reduced on the roof of the vehicle, which creates flow separation and thus turbulence such the C-Pillar vortex starts to generate at the rear of the vehicle. In figure 35 and 36 a steady flow velocity is noticed across the roof of the vehicle, as well as a more uniform wake region. This streamline comparison agrees with the results from figures 21,22, and 23, where the vortex generated with the implementation of passive air injection is weaker in comparison to the base Ahmed model. Additionally a sudden streamline velocity increase is noticed over the 25-degree slant of Design 2, which indicate and agree with a low pressure pocket above the outlets. In figure 35, it is also noticed that the C-pillar vortex is closer to the center of the vehicle than the base Ahmed model, where the vortex with Design 2 is even closer to the center of the vehicle than Design 1.

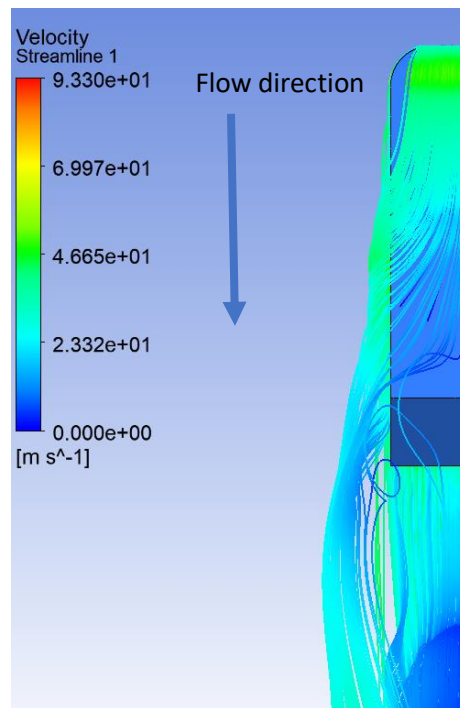


Figure 34 Top-down view of base Ahmed streamline velocity

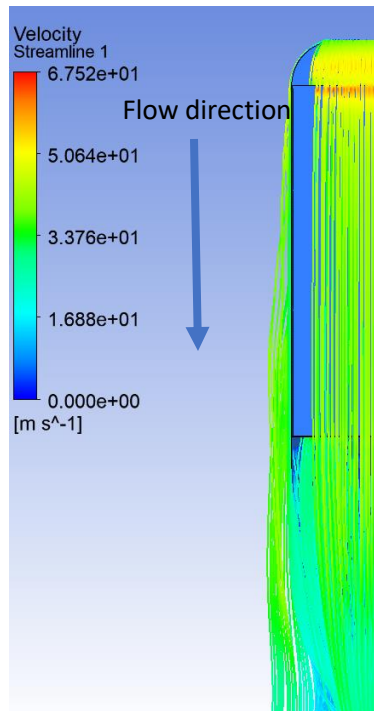


Figure 35 Top-down view of Design 1 streamline velocity

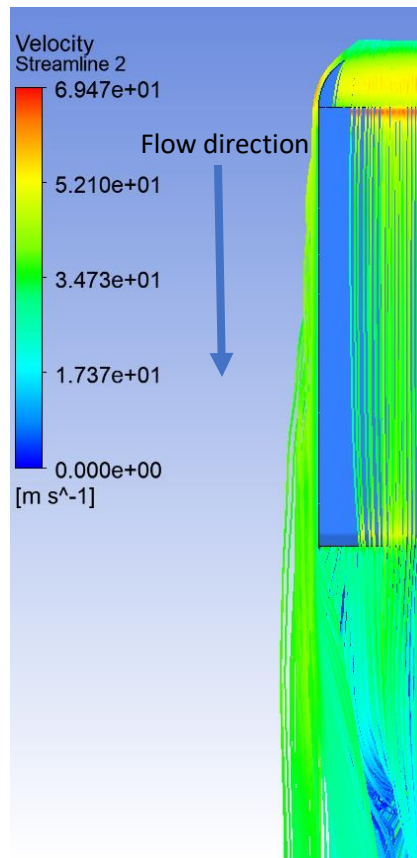


Figure 36 Top-down view of Design 2 streamline velocity

Figures 37,38, and 39 compare the TKE from a top-down view at half height. In this comparison it is further noticed that the wake region of Design 1 is more uniform and controlled when compared to the base Ahmed model. Additionally lower TKE values are noticed in the wake region of Design 1 indicating higher pressures. The implementation of Design 2 resulted in a smaller wake region than both the base Ahmed model as well as Design 1. While the wake region of Design 2 is smaller than Design 1, there a higher TKE values by 39.3% closer to the body of the vehicle, which indicate lower pressures with the implementation of Design 2 that agree with the pressure contours discussed earlier.

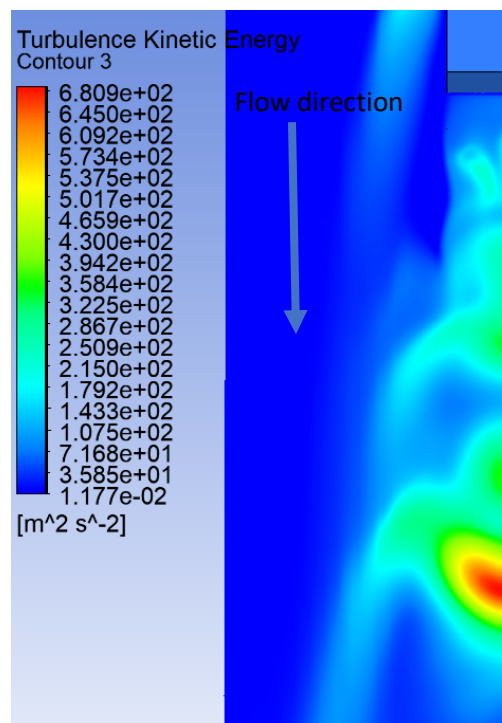


Figure 37 Top-down Turbulence Kinetic Energy of base Ahmed at 0.2m height

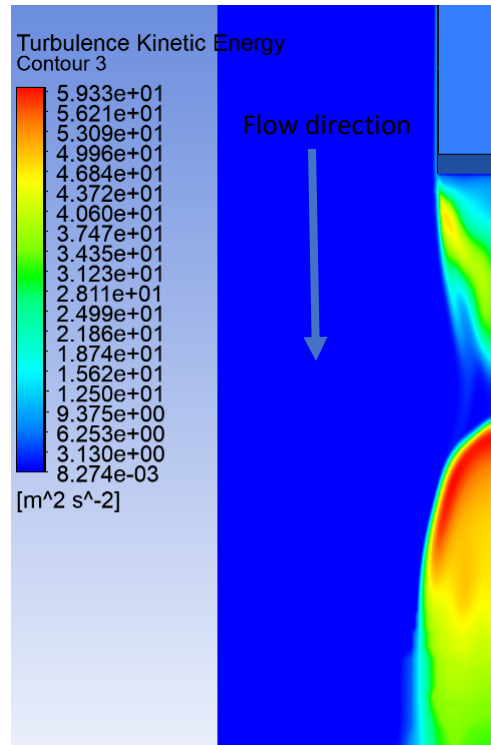


Figure 38 Top-down Turbulence Kinetic Energy of Design 1 at 0.2m height

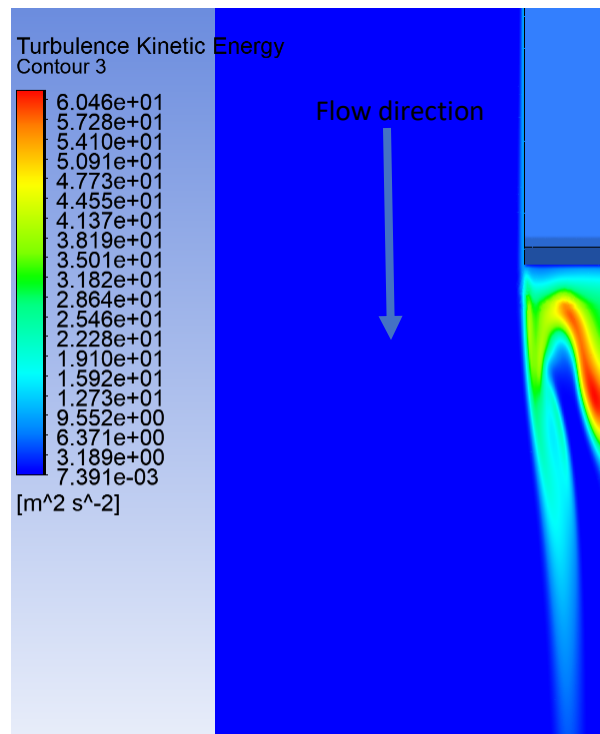


Figure 39 Top-down Turbulence Kinetic Energy of Design 2 at 0.2m height

Figures 41, 42, and 43 compare the TKE at 2 m behind the vehicle, on the plane shown in figure 40, all were in agreement with previous results. The base Ahmed model had larger TKE values, indicating higher turbulence in the wake region than with passive air injection. Additionally, a more uniform distribution is once again observed with the implementation of passive air injection. Where figure 43 agree with the results of a smaller wake region with the implementation of Design 2.

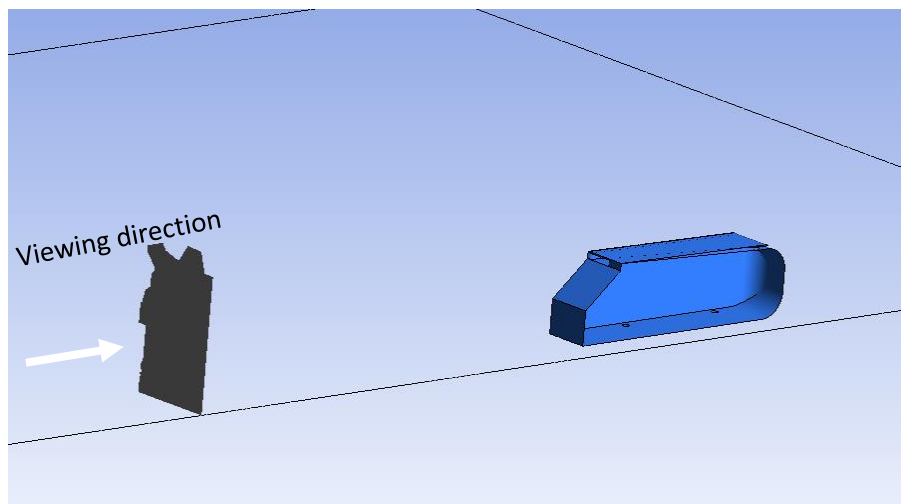


Figure 40 TKE plane location for figures 41-43

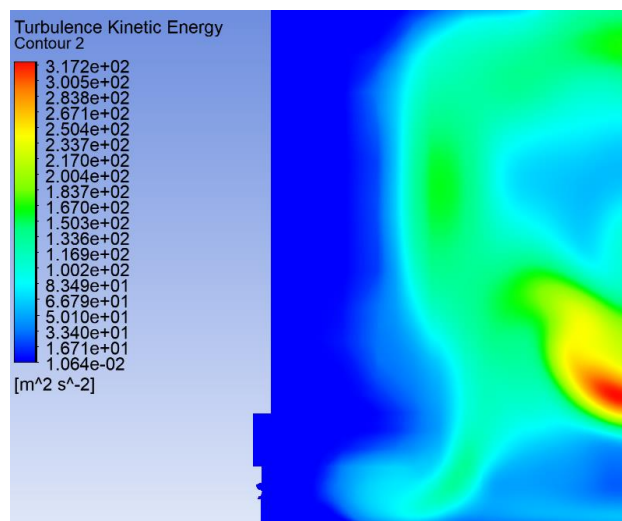


Figure 41 Turbulence Kinetic Energy at -2m behind the base Ahmed model

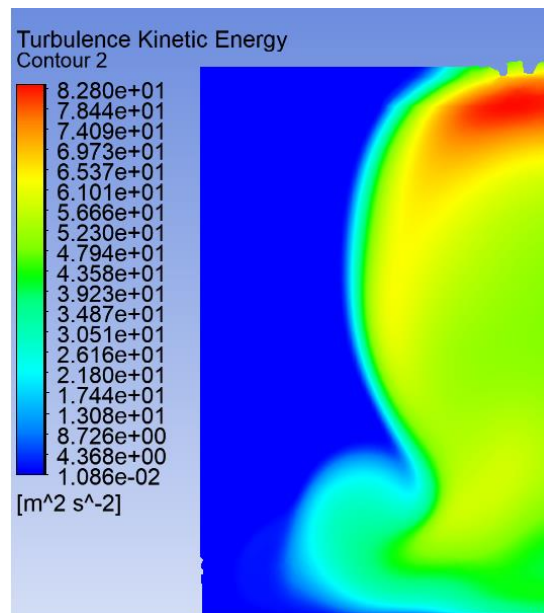


Figure 42 Turbulence Kinetic Energy at -2m behind Design 1

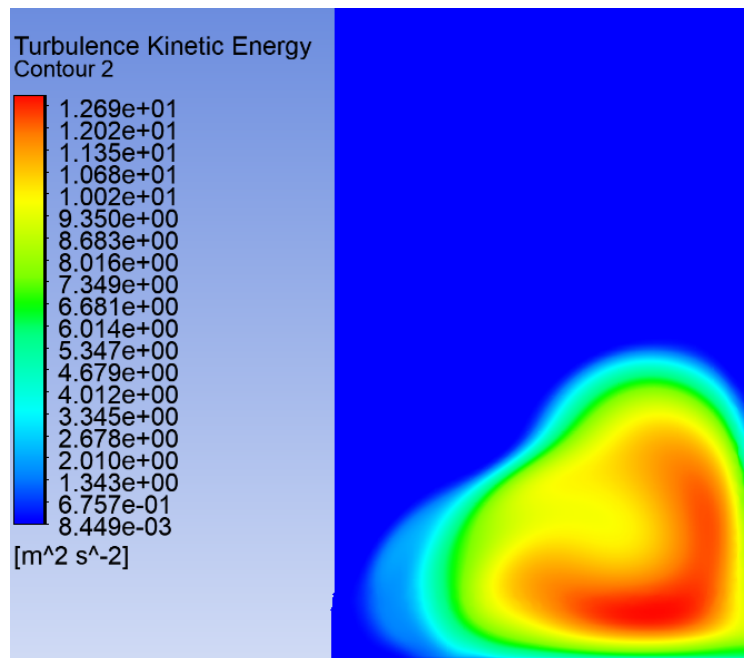


Figure 43 Turbulence Kinetic Energy at -2m behind Design 2

Figures 44 show the inlet Design 1 and Design 2 working, while figure 45 show the outlet of Design 1 and figure 46 show the outlet of Design 2. In figure 44 it is observed that the

high flow air is captured by the inlet and in figures 45 and 46, it is shown that the flow is being injected into the wake region where it has maintained its velocity and is still observed to be laminar flow when exiting the outlet. In figure 46 it is noticed that the formation of the C-pillar vortex has moved to the top edge of the 25-degree slant that was implemented on Design 2, this agrees with figures 19 and 36 that indicated a vortex generation at the outlet of Design 2 that approached the center of the vehicle.

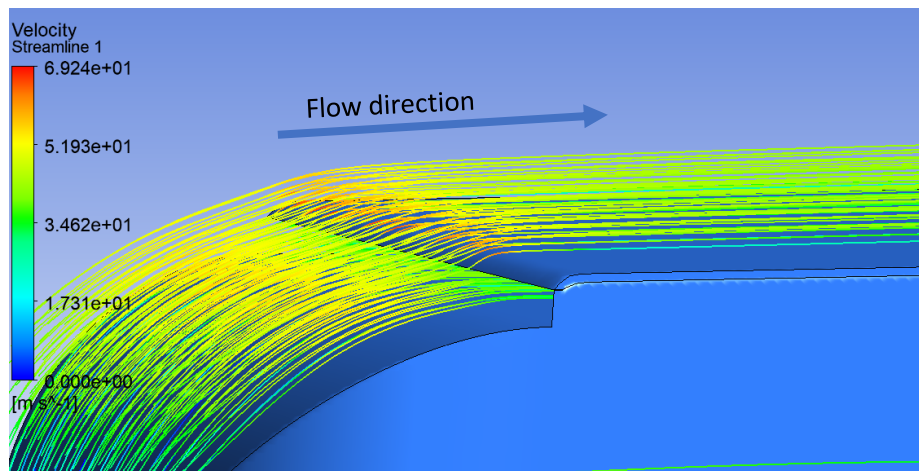


Figure 44 Design 1 inlet Velocity streamlines

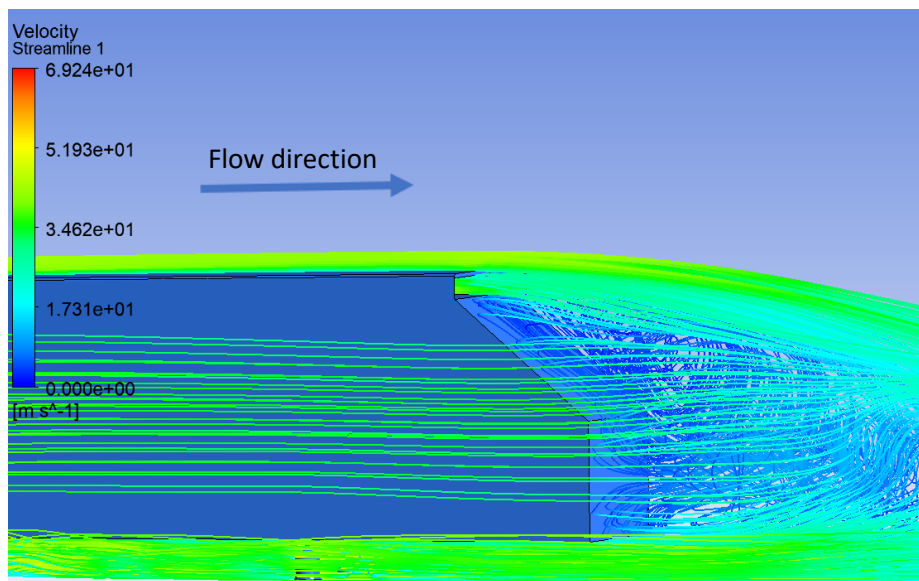


Figure 45 Design 1 outlet velocity streamlines

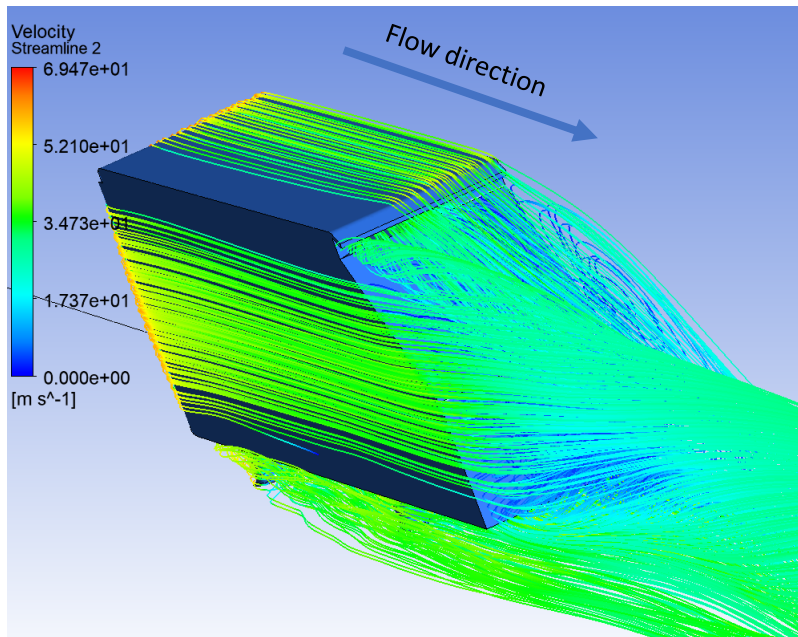


Figure 46 Design 2 outlet velocity streamlines

All results agree by showing overall higher pressures and lower TKE in the wake region of the vehicle with the passive clean air injection, leading to a smaller and weaker wake region. In addition to the smaller wake region and lower pressures, less flow separation is noticed in the top surface of the moving vehicle.

With the increase in the overall pressure in the wake region, the lift coefficient was drastically reduced. As the pressure increased in the wake region, the velocity of the underbody flow was reduced, which in turn increased the pressure under the vehicle, lowering the suction effect.

## Conclusion

The feasibility of a fully passive air injection method was investigated using the standard  $K\omega - SST$  turbulence model and abiding with conservation of mass to maintain the inlet air velocity into the wake region. By implementing a wide inlet, capturing the high velocity air from the front of the moving vehicle was achieved, while the two outlets placed at the rear of the vehicle were able to inject the fluid at the same velocity as the fluid carried at the inlet. This achieved a drag coefficient of  $C_D = 0.282$  at 40m/s, which is an 11% decrease from the base simulation of  $C_D = 0.317$ , and a 5.78% decrease when compared to experimental wind tunnel testing that produced a drag coefficient of  $C_D = 0.299$ . When testing at 20m/s a  $C_D = 0.2883$  was obtained by Design 1, and  $C_D = 0.2895$  was obtained with Design 2, which were an 9.48% and 9.06% reduction when compared to the base Ahmed simulation at 20m/s of  $C_D = 0.3165$ . However, the increase of pressure in the wake region also led to a drastic decrease in the lift coefficient from an experimental  $C_l = 0.345$ , and a simulated  $C_l = 0.37$  to a  $C_l = 0.23$ .

Additionally, by capturing the high velocity air in the inlet, flow separation and turbulence formation that was observed on the roof of the base Ahmed model was avoided. This allowed the pressure on the surface of the vehicle to remain stable allowing the formation of a uniform, tear drop shape, wake region that contained higher pressures. Even though the surface area exposed to fluid flow was increased, it can be ignored as the Ahmed body is a Bluff body dominated by pressure drag, such that any changes to the drag coefficients will be related to the pressure drag and surface drag can be neglected as its contribution will be minimal.

## **Recommendations**

As this thesis focused on the feasibility of a fully passive air injection method, the next step would be to study the flow over a realistic full car model, such as the DrivAer model, and implement Design 1 instead of a half Ahmed Body. This will allow more accurate results and be a final validation if a fully passive air injection system is feasible on the everyday vehicle. In addition to utilizing a realistic full car model, the use of IDDES turbulence model should be used in combination with the model as it has been proven to provide very accurate wake region modeling for the DrivAer model.

Additionally, acoustics research should be conducted to explore any potential vibrations that might be caused in the closed roof venturi design that would result in noise. Such noise would limit the application of this design, as the every day driver would prefer a quiet vehicle cabin.

Another research opportunity of this design would be the implementation on semi-trailers, as downforce and noise is not a concern but pressure drag is, as it will drastically reduce fuel consumption on long highway drives.

## References

- Anderson E, Szewczyk A. 1997. Effects of a splitter plate on the near wake of a circular cylinder in 2 and 3-dimensional flow configurations. *Fluids*23:161–74
- Arcas D, Redekopp L. 2004. Aspects of wake vortex control through base blowing/suction. *Phys. Fluids*16:452–56
- Baek S, Sung HJ. 1998. Numerical simulation of the flow behind a rotary oscillating circular cylinder. *Phys. Fluids*10:869–76
- Bashir, T.A., Soni, A.G., Mahulkar, A.V. and Pandit, A.B. (2011), The CFD driven optimization of a modified venturi for cavitation activity. *Can. J. Chem. Eng.*, 89: 1366-1375. <https://doi.org/10.1002/cjce.20500>
- Barsotti, D. L., Divo, E. A., and Boetcher, S. K. S. (August 6, 2015). "Optimizing Jets for Active Control of Wake Refinement for Ground Vehicles." *ASME. J. Fluids Eng.* December 2015; 137(12): 121108. <https://doi.org/10.1115/1.4030913>
- Brunn, A., Nitsche, W. (2006). Active control of turbulent separated flows over slanted surfaces
- Burk, A. (2014) *Aerodynamik in der frühen Fahrzeugentwicklung*, University of Berlin
- Choi S, Choi H, Kang S. 2002. Characteristics of flow over a rotationally oscillating cylinder at low Reynolds number. *Phys. Fluids*14:2767–77
- Dennis S, Nguyen P, Kocabiyik S. 2000. The flow induced by a rotationally oscillating and translating circular cylinder. *J. Fluid Mech.*407:123–44
- Delaunay Y, Kaiktsis L. 2001. Control of circular cylinder wakes using base mass transpiration. *Phys. Fluids*13:3285–302
- Fujisawa N, Takeda G, Ike N. 2004. Phase-averaged characteristics of flow around a circular cylinder under acoustic excitation control. *J. Fluids Struct.*19:159–70
- Filler J, Marston P, Mih W. 1991. Response of the shear layers separating from a circular cylinder to small-amplitude rotational oscillations. *Fluid Mech.*231:481–99
- Gritskevich S, Mikhail, Garbaruk V, Andrey, Schütze Jochen, Menter R. Florian (2012). Development of DDES and IDDES Formulations for the  $k-\omega$  Shear Stress Transport Model, St. Petersburg State Polytechnical University, DOI 10.1007/s10494-011-9378-4
- Haecheon Choi, Woo-Pyung Jeon, Jinsung Kim, 2008, Control of Flow Over a Bluff Body, School of Mechanical and Aerospace Engineering and Center for Turbulence and Flow Control Research, Institute of Advanced Machinery and Design, Seoul National University, Seoul 151-744, doi:10.1146/annurev.fluid.39.050905.110149
- Hanfeng, W., Mengxia, X. (2012). Control of the aerodynamic drag of an Ahmed model with slot jet

- Hwang J-Y, Yang K-S, Sun S-H. 2003. Reduction of flow-induced forces on a circular cylinder using a detached splitter plate. *Phys. Fluids* 15:2433–36
- Jeon S, Choi J, Jeon W-P, Choi H, Park J. 2004. Active control of flow over a sphere for drag reduction at a subcritical Reynolds number. *J. Fluid Mech.* 517:113–29
- Konstantinidis E, Balabani S, Yianneskis M. 2005. The timing of vortex shedding in a cylinder wake imposed by periodic inflow perturbations. *J. Fluid Mech.* 543:45–55
- Kral, L. D. (2000). Active flow control technology. ASME Fluids Engineering Technical Brief.
- Kwon K, Choi H. 1996. Control of laminar vortex shedding behind a circular cylinder using splitter plates. *Phys. Fluids* 8:479–86
- Leu TS, Ho CM. 2000. Control of global instability in a nonparallel near wake. *J. Fluid Mech.* 404:345–78
- Leighton, T. G., “The Acoustic Bubble,” Academic Press, London, UK (1994).
- Lin J, Towfighi J, Rockwell D. 1995. Near-wake of a circular cylinder: control by steady and unsteady surface injection. *J. Fluids Struct.* 9:659–69
- Mason, T. J., “Practical Sonochemistry: Users Guide to Applications in Chemistry and Chemical Engineering,” Ellis Horwood Series in Organic Chemistry. Ellis Horwood Ltd., Chichester, UK (1992).
- Meile W, Brenn G, Reppenhagen A, Lechner B, Fuchs A, “Experiments and Numerical simulations on the aerodynamics of the Ahmed Body”, 2011
- Nabutola, K. Active drag reduction of ground vehicles using air-jet wheel deflectors Scholarly Commons
- Ozono S. 1999. Flow control of vortex shedding by a short splitter plate asymmetrically arranged downstream of a cylinder. *Phys. Fluids* 11:2928–34
- Poncet P. 2002. Vanishing of mode B in the wake behind a rotationally oscillating circular cylinder. *Phys. Fluids* 14:2021–23
- Poncet P. 2004. Topological aspects of three-dimensional wakes behind rotary oscillating cylinders. *J. Fluid Mech.* 517:27–53
- Princeton . 2022. Drag of Blunt Bodies and streamlined bodies.
- Suzuki, Y., Ijima, T., 1999, Flucome 94, Toulouse
- Sovran, H. Aerodynamics of Road Vehicles, 1993
- Shiels D, Leonard A. 2001. Investigation of a drag reduction on a circular cylinder in rotary oscillation. *J. Fluid Mech.* 431:297–322
- Tokumar PT, Dimotakis PE. 1991. Rotary oscillatory control of a cylinder wake. *J. Fluid Mech.* 224:77–90

Veeralkumar Thakur, Tarun Yadav, Rajiv B. Drag Optimization of Bluff Bodies using CFD for Aerodynamic Applications, International Journal of Computational Engineering Research, ISSN(e):2250-3005, volume 7, issue 4, 2017.

Williams D, Mansy H, Amato C. 1992. The response and symmetry properties of a cylinder wake subjected to localized surface excitation. *J. Fluid Mech.* 234:71–96

Young, F. R., “Cavitation,” McGraw Hill, London, UK (1989).

Zhang, B. F., Liu, K., Zhou, Y., To, S., & Tu, J. Y. (2018). Active drag reduction of a high-drag ahmed body based on steady blowing. *Journal of Fluid Mechanics*, 856, 351-396. doi:<http://dx.doi.org.ezproxy.libproxy.db.erau.edu/10.1017/jfm.2018.703>